

Exploring the potential of Rayleigh-corrected reflectance in coastal and inland water applications: A simple aerosol correction method and its merits

Lian Feng^{a,c,e}, Xuejiao Hou^d, Junsheng Li^{b,*}, Yi Zheng^{a,c,e}

^a State Environmental Protection Key Laboratory of Integrated Surface Water-Groundwater Pollution Control, School of Environmental Science and Engineering, Southern University of Science and Technology, Shenzhen 518055, China

^b Key Laboratory of Digital Earth Science, Institute of Remote Sensing and Digital Earth, Chinese Academy of Sciences, Beijing, China

^c Guangdong Provincial Key Laboratory of Soil and Groundwater Pollution Control, School of Environmental Science and Engineering, Southern University of Science and Technology, Shenzhen 518055, China

^d State Key Laboratory of Information Engineering in Surveying, Mapping and Remote Sensing, Wuhan University, Wuhan 430079, China

^e Shenzhen Municipal Engineering Lab of Environmental IoT Technologies, Shenzhen 518055, China



ARTICLE INFO

Keywords:

MODIS
Surface reflectance
 R_{rc}
Atmospheric correction
Ocean color
Shortwave infrared

ABSTRACT

Atmospheric correction methods that are designed for either ocean color or land applications often result in low-quality or even no surface reflectance data for coastal and inland waters. In contrast, Rayleigh-corrected reflectance (R_{rc}) has been used in water applications, although without removing aerosol scattering. However, a systematic effort has not been made to investigate the uncertainties and applicability of R_{rc} in ocean color studies. This knowledge gap was filled in this study by using Moderate Resolution Imaging Spectroradiometer (MODIS) data covering a large area (almost the entire middle and lower reaches of the Yangtze River Basin and the Yangtze River Estuary) between 2002 and 2016. We first examined the correlation between a quality-controlled reflectance product that was generated using a shortwave-infrared (SWIR)-based atmospheric correction method (R_{rs_swir}) and R_{rc} . Improved relationships between these two products were found for all MODIS bands if a subtraction of the Rayleigh-corrected reflectance at 1240-nm was utilized as the aerosol correction for R_{rc} (R_{rc_1240}). The robust correlations between the two products allow for R_{rs_swir} to be replaced with R_{rc_1240} -converted reflectance (denoted as $R_{rs_rrc_1240}$) in water applications. In situ validations further demonstrated that the accuracy levels between usable $R_{rs_rrc_1240}$ and R_{rs_swir} data are comparable for most MODIS wavelengths. The most striking superiority of $R_{rs_rrc_1240}$ over R_{rs_swir} is the pronounced increase in data coverage (especially for small water bodies), where the percentages of usable observations (PUOs) of the former are several times to more than one order of magnitude higher than those of the latter. The differences in PUOs were mostly due to perturbations related to land adjacency effects (LAEs) in the SWIR-based atmospheric correction. Such effects could also explain the reduced PUOs for smaller water bodies. Ocean color applications in the examined regions could benefit from such a dramatic increase in PUOs, which could enhance the capability of tracking short- to long-term dynamics and could create new possibilities for inland water system monitoring at the basin scale.

1. Introduction

Over the past several decades, significant progress has been made in research on coastal and inland waters by utilizing satellite ocean color remote sensing to quantitatively measure water quality parameters (such as the concentrations of total suspended sediment (TSS) and chlorophyll-a (Chl-a)) (Budhiman et al., 2012; Son and Kim, 2018) and to understand the impacts of climatic changes and/or human activities on the ecological and biogeochemical functions of water bodies. However, many challenges have remained unresolved for decades (Mouw

et al., 2015), one of which is the lack of an accurate surface reflectance product, leading to a lack of data or low-quality inputs for various inversion algorithms that are used for water quality product retrievals.

The difficulties associated with atmospheric correction over optically complex coastal and inland waters are the primary reasons for this challenge. The atmospheric path radiance received by a sensor at the top-of-atmosphere (TOA) can be mainly decomposed into Rayleigh and aerosol scattering. While the Rayleigh component can be computed accurately even with the consideration of polarization effects (Gordon, 1997), the estimation of aerosol reflection is difficult. The classic

* Corresponding author.

E-mail address: lij@radi.ac.cn (J. Li).

atmospheric correction (AC) algorithm for Moderate Resolution Imaging Spectroradiometer (MODIS) imagery often fails in coastal and inland waters, yielding negative reflectance due to overcorrections and leading to large errors to the derived ocean color products (Gordon, 1997; Gordon and Wang, 1994; Hu et al., 2000; Ruddick et al., 2000). These errors mainly occur because the black-pixel assumption in the near-infrared (NIR) bands is not valid in turbid waters because of the elevated signals in the NIR bands associated with significant particle scattering. An additional challenge for the NIR-based method is signal saturation over highly reflective waters (Hu et al., 2012), which further limits the validity of R_{rs} products.

Algorithms have also been developed to tackle non-“black-pixel” issues, including but not limited to spatial extrapolation of aerosol information from nearby clear waters, assumptions of spectral shape in aerosol scattering, relationship between Chl-a concentration and NIR reflection (Hu et al., 2000; Jamet et al., 2011; Ruddick et al., 2000; Siegel et al., 2000; Stumpf et al., 2003) and the replacement of the original NIR bands with the shortwave-infrared (SWIR) wavelengths (Novoa et al., 2017; Vanhelmont and Ruddick, 2015; Wang and Shi, 2007). The last approach has been implemented as an alternative algorithm in both NASA's and NOAA's software package SeaDAS to derive R_{rs} products for coastal and inland productive waters (denoted as R_{rs_swir}).

Theoretically, water reflection in SWIR bands is essentially zero, even for extremely turbid waters, because the water absorption coefficients are significantly higher for these bands than for NIR bands (Hale and Querry, 1973), and the TOA signal in the SWIR wavelengths is the result of the atmospheric path radiance. Therefore, the surface reflectance estimation from the SWIR-based AC method is expected to be reliable, as long as the absorbing aerosol is not dominant in the atmosphere (Chander et al., 2009) and the SWIR bands have sufficient signal-to-noise ratios (Hu et al., 2012). Indeed, this AC approach has demonstrated promising performance in producing satisfactory remote sensing reflectance (R_{rs} , in sr^{-1}) values, even in the most turbid waters, such as the Yangtze River Estuary where the TSS concentrations reach $> 1000 \text{ mg L}^{-1}$ (Wang et al., 2007). The uncertainties in the resulting R_{rs} values could be significantly reduced through various radiometric calibration and noise reduction schemes for SWIR bands (Li et al., 2017).

Currently, the use of R_{rs_swir} in coastal and inland waters suffers from several limitations. The first limitation is the contamination of land adjacency effects (LAEs). Due to the significant reflectance contrast between land and water, the radiance of the nearby “bright” land pixels scatter into the field of view of the satellite instruments, enhancing the signals of water pixels. The LAEs tend to increase with increasing wavelength, leading to large uncertainties in the two candidate SWIR AC bands and thus providing problematic R_{rs_swir} retrievals. Indeed, these effects could extend several kilometers from the coastline, resulting in erroneous surface reflectance results within this distance. The second limiting factor is that the SWIR AC approach embedded in SeaDAS often fails without valid R_{rs} outputs, especially when applied to relatively small water bodies (see results below). Even after adjustments to the default processing options (e.g., turning off the masks for land, shallow water, and sunglint and raising the default thresholds for aerosol optical thickness and cloud albedo), this data loss problem is still prominent.

Due to the lack of R_{rs} produced with the ocean color-based AC algorithms (either NIR- or SWIR-based AC methods), other reflectance products are often selected for coastal and inland waters applications. For example, MODIS land surface reflectance products (MYD09 for Aqua and MOD09 for Terra, denoted as R_{Land}), which are generated using the land-oriented AC approach (Kaufman et al., 1997), have been proven to be applicable to water turbidity mapping in many estuaries and inland lakes (Hou et al., 2017; Li et al., 2016; Petus et al., 2010, 2014; Zhang et al., 2014). A recent study by Feng et al. (2018) also demonstrated the high accuracies of $R_{Land}(645)$ and $R_{Land}(645/$

555). However, spatial patchiness over water surfaces has been observed in R_{Land} products, largely because a 10×10 pixel (1-km resolution) moving window is utilized during aerosol correction (Kaufman et al., 1997). Although a spatial and temporal binning scheme has been recommended to minimize the patchiness noise in R_{Land} images (Feng et al., 2018), it sacrifices the original spatial and temporal resolutions.

Surface reflectance products that are derived using AC processes designed for either ocean color (based on NIR or SWIR) or land applications are very sensitive to environmental disturbance (such as LAEs), leading to low-quality data (e.g., noisy or negative) or even no data coverage in coastal and inland waters. As the interferences generally occur in the aerosol correction procedures, a natural question would be whether the Rayleigh-corrected reflectance (R_{rc} , dimensionless) is sufficiently accurate without an aerosol removal step for ocean color studies. Indeed, R_{rc} has been proven to be useful for estuaries and inland water investigations in a number of pioneering studies (Duan et al., 2014; Feng et al., 2014b; Markham et al., 2008; Zhang et al., 2016), and R_{rc} even produced higher quality images with less noise and spatial patchiness than the R_{Land} and R_{rs_swir} products (Feng et al., 2018).

However, to date, a systematic effort has not been made to assess the consistency between R_{rc} and different reflectance products, and the uncertainties and general applicability of R_{rc} in water applications are generally unknown, not to mention the fidelity of the derived water properties. The current study is thus designed to fill this knowledge gap and to provide a general guideline for the use of R_{rc} in coastal and inland water studies. In detail, this study has the following objectives:

- (1) Examine the consistency between R_{rc} and R_{rs_swir} , where the quality of R_{rs_swir} is assessed using an objective quality assurance system.
- (2) Identify the relationships between the two different products for various MODIS bands and demonstrate the superiority of R_{rc} -converted reflectance in data coverage.
- (3) Assess the impacts of land adjacency on the data coverage of R_{rc} -converted reflectance and discuss the limitations of this method and its implications for ocean color applications.

2. Datasets and preprocessing

2.1. Remote sensing datasets

MODIS Aqua Level-1A Local-Area-Coverage (LAC) data were downloaded from the NASA Goddard Space Flight Center (GSFC, <https://oceancolor.gsfc.nasa.gov/>). To allow full coverage of different weather (aerosol) conditions, water characteristics, and solar/viewing geometries, all available data between July 2002 and December 2016 that covered all of region 1 (the lower reaches of Yangtze River Basin, the Yangtze River Estuary and adjacent ocean areas) and region 2 (the middle reaches of the Yangtze River Basin) (see locations in Fig. 1) were obtained. Both regions contain many lakes, river channels and/or coastal ocean areas, while the water bodies in region 1 are generally larger than those in region 2. The MODIS data were then processed with the l2_gen module of the SeaDAS software (version 7.3) to generate two reflectance product types.

The first reflectance product is the Rayleigh-corrected reflectance (R_{rc} , dimensionless) (Hu, 2009), where the Rayleigh (molecular) scattering effects are removed, leaving the aerosol contributions in the data products. This partial AC can be expressed as:

$$R_{rc} = \pi L_t^*/(F_0 \times \cos \theta_0) - R_r \quad (1)$$

where F_0 is the extraterrestrial solar irradiance, θ_0 is the solar zenith angle, L_t^* is the radiometrically calibrated at-sensor radiance after removing the gaseous absorption, and R_r is the reflectance due to Rayleigh (molecular) scattering.

The second product is the fully atmospherically corrected remote sensing reflectance (i.e., R_{rs}), where the contributions of both Rayleigh

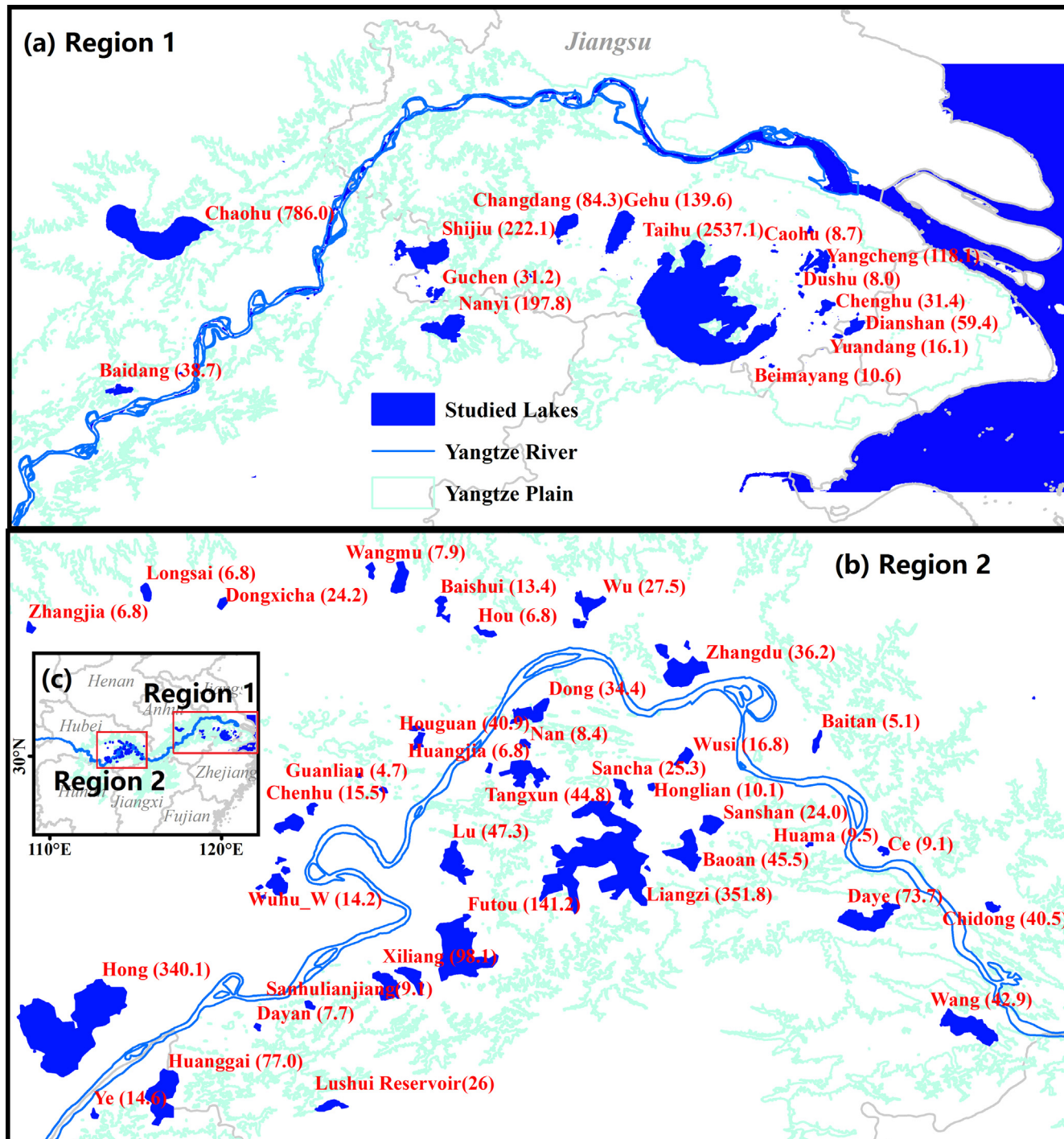


Fig. 1. Locations of the study regions. The areas shaded in blue are the water bodies examined in this study, including lakes (the names and surface areas (in km²) are noted), the Yangtze River channel and the Yangtze Estuary. Green lines show the boundary of the Yangtze Plain.

and aerosol scattering to the satellite signal have been removed, and the aerosol scattering correction is conducted with the SWIR-based AC method (Wang and Shi, 2007). Due to the frequent presence of high aerosol concentrations and the extremely high water turbidity in the study region (Feng et al., 2014a), the default cloud albedo mask was changed from $R_{rc, 869} = 2.7\%$ to $R_{rc, 2130} = 3.7\%$ (Wang and Shi, 2006; Zhang et al., 2014). Otherwise, a substantial amount of cloud-free satellite observations could be masked without any reflectance retrievals. The masking keywords of “maskland” (mask out all land pixels) and “maskbath” (mask out shallow water) in the l2_gen module were turned off to maximize the coverage of the R_{rs} retrievals. In addition, a median

filter was applied before conducting the AC process to remove noise and improve the signal-to-noise ratio (SNR) of the two candidate bands for AC (centered at 1240 nm and 2130 nm).

Reflectance products were generated for all visible to NIR MODIS bands, including nine 1-km resolution ocean bands (i.e., 412, 443, 488, 531, 547, 667, 678, 748, and 869 nm, originally designed for ocean color applications) and four land bands (645 and 859 nm with 250-m resolution, and 469 and 555 nm with 500-m resolution, originally designed for land-based applications). These data were projected to the same cylindrical equidistance (rectangular) projection and were resampled to 250-m resolution to facilitate further comparisons and

validations. During the generation of these reflectance products, the 32-bit quality control flags (l2_flags) associated with each pixel were also generated and recorded (<https://oceancolor.gsfc.nasa.gov/atbd/ocl2flags/>), which were then used to discard low-quality data for subsequent comparisons, such as cloud presence and stray-light contamination.

2.2. In situ data

Spectral reflectance data of several lakes (including Shijiu Lake, Yangcheng Lake, Chenghu Lake, Taihu Lake, and Chaohu Lake in region 1 and Hong Lake and Liangzi Lake in region 2) and the Yangtze River Estuary (in region 1) were collected between 2005 and 2018, yielding > 800 total samples. These field surveys were conducted across different seasons (Li et al., 2017), representing diverse water and aerosol properties. The R_{rs} data were acquired with FieldSpec (manufactured by Analytical Spectral Device, ASD) or PSR + 3500 (manufactured by Spectral Evolution) field-portable spectrometers, and some of these datasets have been extensively used in previous works to study the bio-optical features of the regions (Sun et al., 2013; Zhang et al., 2008, 2015). The Ocean Optics protocol recommended by NASA for above-water spectral measurements was followed when collecting the field data (Mobley, 1999; Mueller et al., 2003), and this protocol can be briefly described as follows: the downward sky radiance (L_{sky}), upward radiance (L_u) and radiance from a standard reference plaque (L_p) were measured for each spectral measurement, and the remote sensing reflectance was then calculated as:

$$R_{rs} = \rho_p (L_u - \rho_f \times L_{sky}) / \pi L_p \quad (2)$$

where ρ_f is the reflection of sky light on water surface, which was assumed to be 0.022. ρ_p is the reflectance of the plaque provided by the manufacturer.

Concurrent satellite and in situ reflectance matchups were also obtained, and several quality control criteria were applied: (1) the satellite and in situ measurements must have a time difference of < 3 h (Bailey and Werdell, 2006) to avoid changes in the water properties and (2) a homogeneity test is utilized to eliminate significant spatial disparities between the MODIS (250-m ~ 1-km spatial resolution) and in situ (a single point) data. When the coefficient of variation (i.e., standard deviation/mean) of the 3×3 MODIS pixel window centered on the in situ point was > 0.4, the data were not selected for matchups (Harding et al., 2005).

3. Methods

3.1. Correlation analysis between Best-Quality R_{rs} and R_{rc}

Ideally, in situ measured R_{rs} and concurrent remotely sensed R_{rc} should be used to test how aerosol correction influences R_{rs} and to examine the potential relationships between R_{rs} and R_{rc} . However, due to the difficulties in obtaining field R_{rs} (the process requires considerable time and labor) and the frequent presence of clouds in the study region, it is challenging to collect sufficient datasets to establish robust correlations between these two types of reflectance products, not to mention the data coverage limitations among different atmospheric/water conditions, observational/solar geometries, etc. On the other hand, although satellite-derived $R_{rs,swir}$ has been demonstrated to be reliable in coastal and inland productive waters through extensive validations, its performance could also be affected. For example, the accuracies in blue bands appeared to be lower than those in red and NIR bands, which is primarily due to the longer extrapolation distances from the SWIR bands (Li et al., 2017). In addition, owing to the significant contrasts between water and land signals, the SWIR bands are prone to LAEs, stray light, etc., prorogating uncertainties into the retrieved R_{rs} (Feng and Hu, 2016, 2017). Therefore, additional processes

are required to circumvent the interference of those residual errors on the relationship between R_{rs} and R_{rc} .

To ensure the high quality of the fully atmospherically corrected R_{rs} (i.e., $R_{rs,swir}$), a recently developed objective quality assurance (QA) system was applied (Wei et al., 2016). While the details of this system can be found in Wei et al. (2016), it can be briefly summarized as follows: the QA system has reference spectra and associated upper/lower bounds for 23 optical water types, ranging from clear blue waters to turbid yellow waters. The system compares the spectral shape of the examined R_{rs} with the reference spectra, and a score between 0 and 1 is assigned according to the agreements for each band, with 1 representing a perfect R_{rs} and 0 representing the worst and unusable R_{rs} . Then, the mean score for all available bands is estimated to represent the score for the target R_{rs} spectrum. The QA system has been demonstrated to be very useful for identifying questionable and likely erroneous spectra (Wei et al., 2016). However, the QA system was developed based on the NASA bio-Optical Marine Algorithm Dataset (NOMAD) (Werdell and Bailey, 2005), and its uses for water types beyond this dataset could be problematic. Additionally, the QA system works only for blue to red bands, and predefined reference spectra and the associated upper/lower bounds for longer wavelengths are not available (Wei et al., 2016).

A score threshold of 0.9 was used to determine the Best-Quality $R_{rs,swir}$ for four land bands (469, 555, 645, and 859 nm) and five blue-to-green ocean bands (412, 443, 488, 531, and 547 nm). Due to the easy saturation nature of the remaining ocean bands (667, 678, 748 and 869 nm, with a saturation rate of more than 60% in Taihu Lake) (Li et al., 2017), a relaxed threshold of 0.85 was used to ensure sufficient data points to establish statistically significant relationships between $R_{rs,swir}$ and R_{rc} . A sensitivity analysis of thresholds of 0.95, 0.9, 0.85 and 0.8 confirmed that the resulting correlations were very similar to those shown in Figs. 2 and 3, and the use of 0.9 and 0.85 for different MODIS bands represents a compromise between data availability and $R_{rs,swir}$ quality. Then, the Best-Quality $R_{rs,swir}$ retrievals for the lakes in regions 1 and 2 covering the period of 2002–2016 were selected with the aforementioned scoring method and were plotted against the corresponding R_{rc} data to construct the correlations between these two types of reflectance products.

To examine whether a simple aerosol correction of R_{rc} could improve its correlation with $R_{rs,swir}$, the differences between R_{rc} , λ (where λ represents the different MODIS bands in the blue to NIR spectral regions) and $R_{rc,1240}$ (denoted as $R_{rc-1240}$) were estimated (Feng et al., 2012). The theoretical basis of this processing step is that the water reflectance at 1240 nm is zero due to the extremely high water absorption, and $R_{rc,1240}$ can be safely assumed to be an aerosol scattering effect. As such, $R_{rc-1240}$ can be regarded as a partial aerosol correction, although full aerosol removal requires consideration of the spectral dependency of aerosol scattering.

The R_{rs} spectrum has a QA score greater than 0.5; that is, half of the MODIS bands fall within the lower/upper bounds of the 23 waters types, and this spectrum was considered the usable data in this study (the same definition as in Wei et al. (2016)). In contrast, an R_{rs} spectrum with a score of < 0.5 is considered to consist of low-quality data that cannot be used for ocean color applications.

3.2. Comparisons of the PUOs

Numerically, R_{rc} can be converted into $R_{rs,swir}$ (denoted as $R_{rs,rrc}$) using the above-established correlations. In practice, all MODIS R_{rc} products over both regions were converted into $R_{rs,rrc}$. Then, for each MODIS $R_{rs,rrc}$ spectrum, the QA system was also applied to gauge its performance, as was previously conducted for $R_{rs,swir}$ when selecting the Best-Quality spectrum.

The usable R_{rs} spectra for both $R_{rs,rrc}$ and $R_{rs,swir}$ were selected from all processed MODIS data between 2002 and 2016 and were then used to calculate the percentage of usable observations (PUOs). The PUOs is

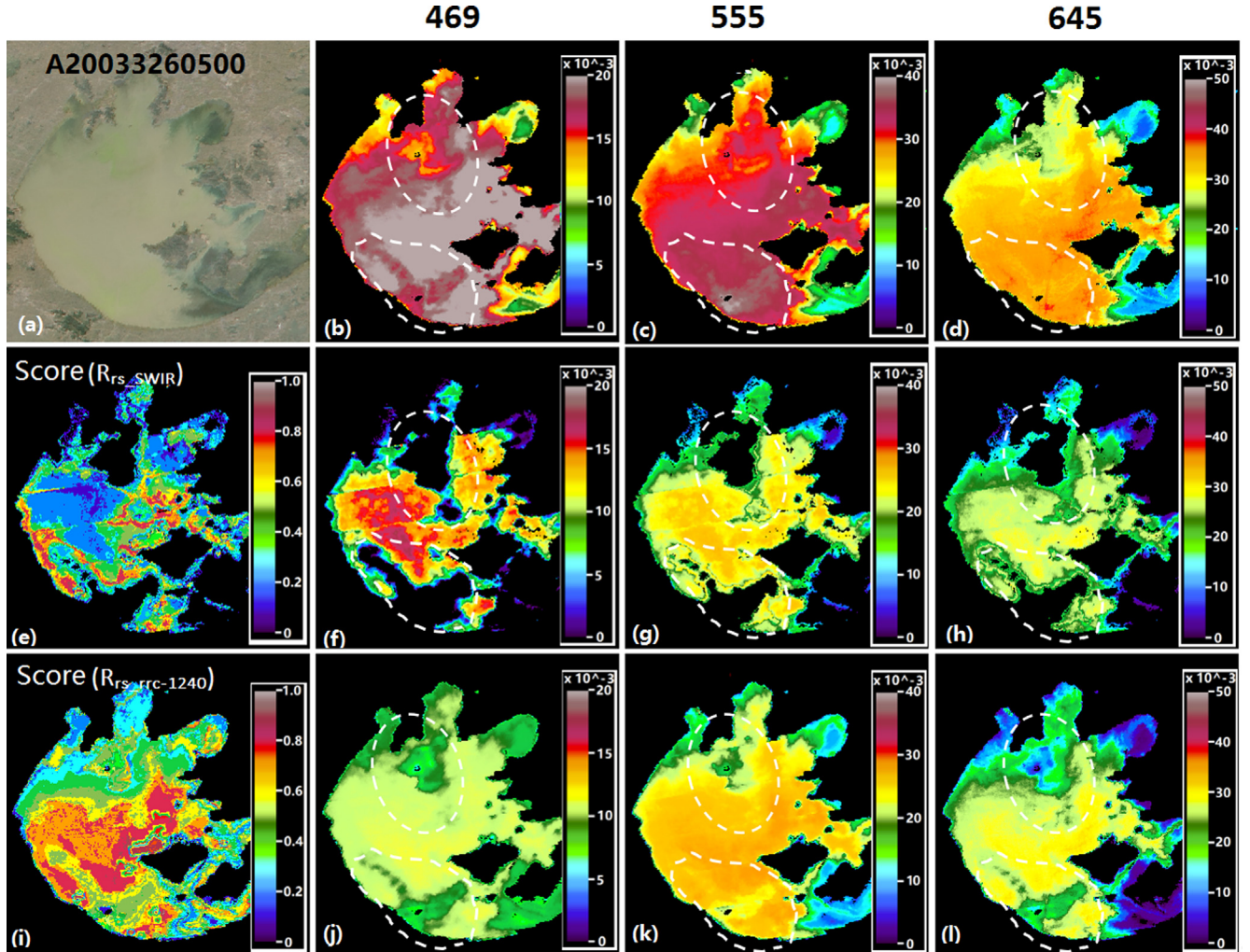


Fig. 2. Scatter plots between R_{rs_swir} and R_{rc_1240} for nine MODIS ocean bands; the R^2 and RMSD values between the two datasets are also noted. Blue, green and red represent the data points from 2005, 2010 and 2015, respectively. The points from the three color-coded years could not be distinguished from the other years, and the associated correlations were very similar to those of the full dataset.

defined as the ratio between the number of usable R_{rs} spectra and the total number of satellite observations within a certain period and represents the possibility of MODIS obtaining usable R_{rs} spectra. The PUs calculations were conducted for the entire period and different climatological seasons. The disparities between the PUs of R_{rs_rrc} and R_{rs_swir} were estimated in terms of different time periods and regions.

3.3. Validations using *in situ* spectral measurements

In situ measured reflectance data were used to gauge the performance of usable $R_{rs_rrc-1240}$. Matched pairs of usable $R_{rs_rrc-1240}$ and field-measured R_{rs} data were first selected using the QA scoring system (Wei et al., 2016) and statistical measures, including R^2 , root mean square difference (RMSD), mean and median ratios. In addition, these accuracy measures for R_{rs_swir} were estimated using the same points used to measure the accuracy of $R_{rs_rrc-1240}$.

4. Results

4.1. Correlations between R_{rs_swir} and R_{rc} for different MODIS bands

Comparisons between R_{rs_swir} and R_{rc} for several bands of a typical MODIS image collected on November 11, 2013, are shown in Fig. 4. The R_{rc} data were divided by π (denoted $R_{rc/\pi}$) to match R_{rs_swir} to allow a direct comparison between different reflectance products. $R_{rc/\pi}$ showed

much higher values than R_{rs_swir} for all spectral bands (especially for short wavelengths) due to the remaining aerosol radiance. The R_{rs_swir} images appeared to be noisier than $R_{rc/\pi}$ images, which can be attributed to the use of low-SNR SWIR bands (1240 and 2130-nm) for aerosol correction (Wang and Shi, 2012). Other than the disparities in the data magnitudes, the most significant difference between these two products is data coverage. Several sections in northern and southern Taihu Lake (circled in white) showed no data in three ocean bands using R_{rs_swir} , while valid $R_{rc/\pi}$ retrievals were found in those regions. The missing R_{rs_swir} data are likely due to failures in the SWIR-based AC process, which are associated with problems such as LAE, stray-light contamination, and erroneous aerosol extrapolations. These problems are more acute in smaller lakes, leading to the drastically reduced data coverage.

Scatter plots of the MODIS R_{rs_swir} and R_{rc} data that passed the QA system as Best-Quality datasets are provided in Fig. S1 (ocean bands) and Fig. S2 (land bands). The negative values in several NIR wavelengths are likely attributed to the lack of reference spectra in the QA system for these bands. In terms of the coefficient of determination (i.e., R^2), these two products showed high agreements for the red-to-NIR bands ($R^2 > 0.5$), while lower agreements were observed in the shorter wavelengths (blue-to-green bands), with R^2 values of generally < 0.5 . The RMSD values between R_{rs_swir} and R_{rc} -estimated R_{rs} (R_{rs_rrc}) ranged between 10.8% for the 555-nm band and 51.0% for the 859-nm band. The differences between R_{rs_swir} and R_{rs_rrc} appeared to be

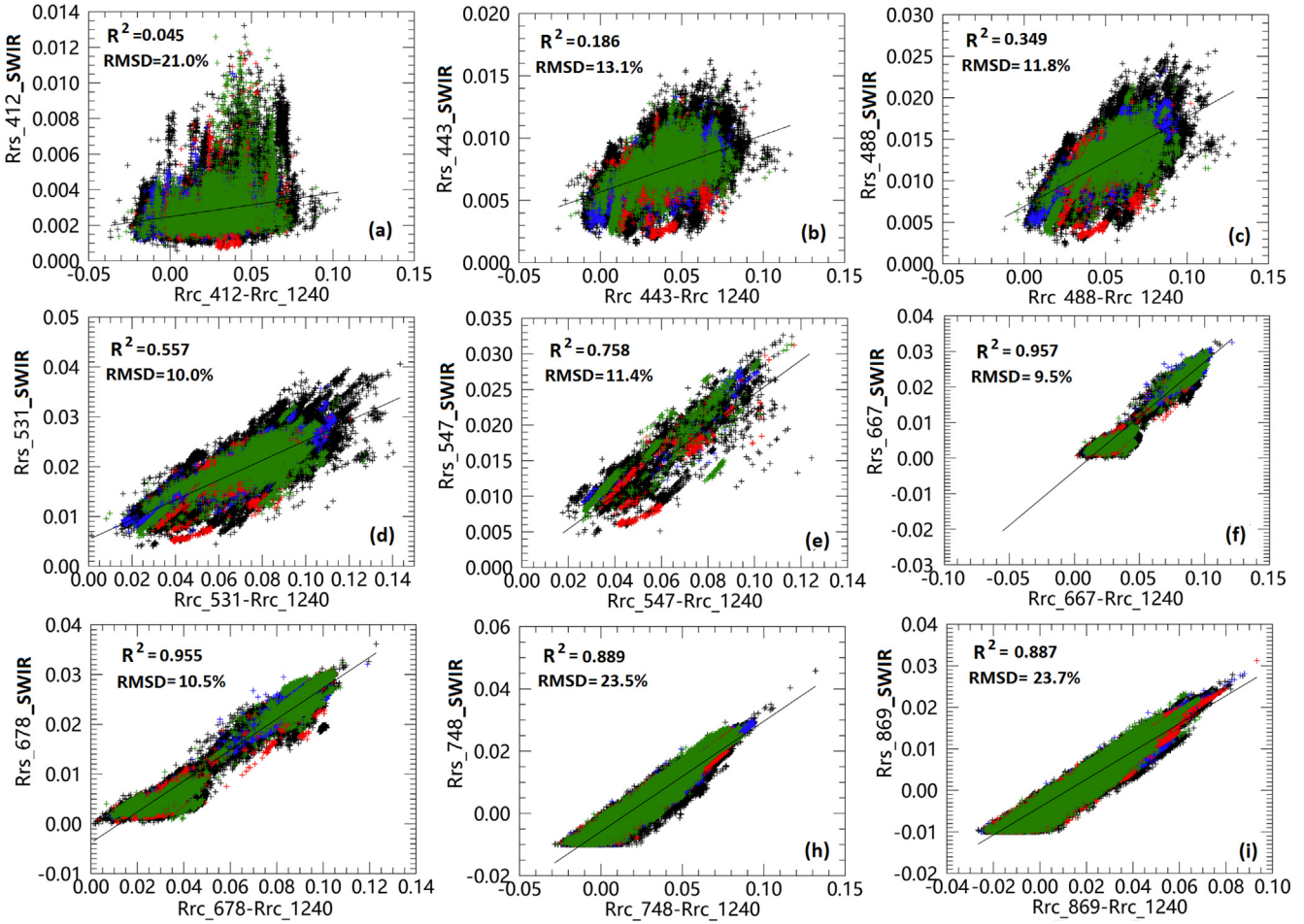


Fig. 3. Same as Fig. 2, but the data are from the four MODIS land bands.

linked with the uncorrected aerosol signal in R_{rc} , while these effects were removed from R_{rs_swir} through the SWIR-based AC method.

The correlations between Best-Quality R_{rs_swir} and $R_{rc-1240}$ for

MODIS ocean- and land- bands are illustrated in Figs. 2 and 3, respectively. Compared with the relationships between R_{rs_swir} and R_{rc} , a simple aerosol correction of R_{rc} (i.e., $R_{rc-1240}$) substantially improved

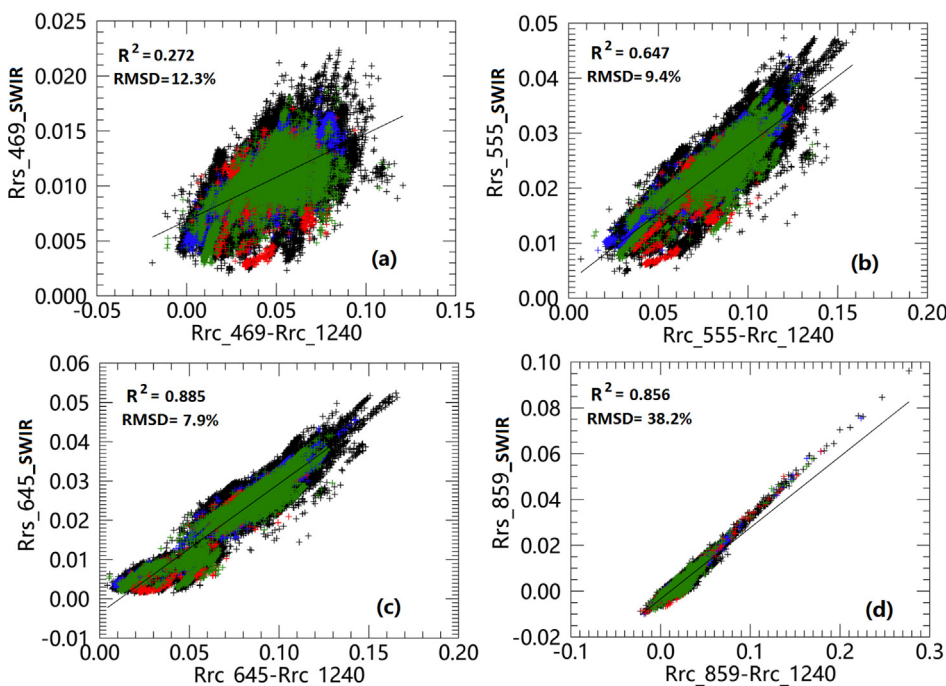


Fig. 4. The comparisons between R_{rc} (b-d), R_{rs_swir} (g-h), and $R_{rc_rss-1240}$ (j-l) for three land bands of one typical MODIS image collected on November 11, 2013. (a) The corresponding RGB composite. The R_{rc} values were divided by π to match the other two products. The areas circled in white clearly demonstrate the missing data problem of R_{rs_swir} . The quality assurance scores for R_{rs_swir} and $R_{rc_rss-1240}$ are shown in (e) and (f), respectively, and the improved quality of $R_{rc_rss-1240}$ is obvious.

Table 1

The regression correlations established using the Best-Quality R_{rs_swir} (Y) and $R_{rc-1240}$ (X) products; the scatter plots are shown in Figs. 2 and 3. Uncertainty measures (RMSD, R^2 , mean/median ratios) between the R_{rs_swir} and $R_{rs_rrc-1240}$ were estimated and are listed. The last column shows the number of points used to establish the relationship between R_{rs_swir} and $R_{rc-1240}$.

Wavelength	Equation	RMSD (%)	R^2	Mean Ratio	Median Ratio	n_points
412	$Y = 0.00248485 + 0.0133166X$	21.0	0.045	1.11	1.08	159,294
443	$Y = 0.00566803 + 0.0457999X$	13.1	0.186	1.06	0.99	159,294
469	$Y = 0.00684795 + 0.0789511X$	12.3	0.272	1.06	0.99	159,294
488	$Y = 0.00693808 + 0.107473X$	11.8	0.349	1.05	0.99	159,294
531	$Y = 0.00539041 + 0.198393X$	10.0	0.557	1.03	0.99	14,979
547	$Y = 0.00065701 + 0.237217X$	11.4	0.758	1.04	0.99	159,294
555	$Y = 0.00296761 + 0.249262X$	9.4	0.647	1.03	0.99	159,294
645	$Y = -0.00368113 + 0.330055X$	7.9	0.882	1.04	0.98	159,294
667	$Y = -0.00374227 + 0.308157X$	9.5	0.957	45.23	0.98	90,431
678	$Y = -0.00400074 + 0.313065X$	10.5	0.955	1.00	0.98	113,183
748	$Y = -0.00580124 + 0.353910X$	23.5	0.889	-143.00	0.94	968,836
859	$Y = -0.00340528 + 0.310890X$	38.2	0.856	220.15	0.82	159,287
869	$Y = -0.00403771 + 0.335256X$	23.7	0.887	-37.62	0.95	126,642

the agreements with R_{rs_swir} for all MODIS bands, as demonstrated by the tighter clustering in the scatter plots, higher R^2 values and lower RMSD values. Table 1 shows the regression correlations between R_{rs_swir} and $R_{rc-1240}$ and the accuracy measures between Best-Quality R_{rs_swir} and $R_{rc-1240}$ -estimated R_{rs} (i.e., $R_{rs_rrc-1240}$) (including RMSD and mean/median ratios). Specifically, R^2 values of > 0.5 were found for all MODIS green-to-NIR wavelengths, and the red-to-NIR bands showed even higher R^2 values of > 0.85 . The RMSD values between R_{rs_swir} and $R_{rs_rrc-1240}$ were much smaller than those between R_{rs_swir} and R_{rs_rrc} , with a low value of $< 25\%$ (mostly $< 15\%$, except for 38.2% for the 859-nm band). The consistency between R_{rs_swir} and $R_{rs_rrc-1240}$ was further revealed by the median/mean ratios of ~ 1 (i.e., the mean/median values R_{rs_swir} and $R_{rs_rrc-1240}$ are close to each other) for most of the MODIS bands. In contrast, the large median/mean ratios for several NIR bands may be associated with their extremely low R_{rs_swir} signals. Indeed, when the data from different years are color coded as shown in Figs. 2 and 3 (red: 2015, green: 2010 and blue: 2005), the points from the three different years cannot be distinguished from the other years. Moreover, the associated correlations were very similar to those of the complete datasets, indicating that the relationships between R_{rs_swir} and $R_{rc-1240}$ were consistent. Indeed, $> 10,000$ points (mostly $> 100,000$) were used to establish these correlations, suggesting that the relationships between R_{rs_swir} and $R_{rc-1240}$ are statistically meaningful.

4.2. Higher PUs from $R_{rs_rrc-1240}$ than R_{rs_swir}

The R_{rc} products from region 1 and region 2 during the 15-year observation period were converted into $R_{rs_rrc-1240}$ using the coefficients listed in Table 1, and the QA system was also applied to obtain usable $R_{rs_rrc-1240}$ products, which were then used to estimate the PUs in different time periods. For comparison purposes, the same PUs calculation process was also used for R_{rs_swir} .

The PUs from R_{rs_swir} and $R_{rs_rrc-1240}$ for the entire period (2002–2016) in region 1 are shown in Fig. 5. Generally, the PUs of R_{rs_swir} were $< 5\%$ for the entire region (purplish to bluish), with a mean value of 2.0% (i.e., the arithmetic mean of all valid pixels in this region). This result indicates that for every 100 MODIS Aqua observations, only two images are expected to have usable R_{rs} values when the SWIR-based AC approach is conducted. The probability of obtaining usable R_{rs_swir} is even lower for small water bodies (such as Yangcheng Lake, Shiji Lake, and the Yangtze River channel), where the mean PUs were $< 1\%$. In contrast, the $R_{rs_rrc-1240}$ data showed much higher values than R_{rs_swir} , with a mean PUs of 15% for region 1. Large water bodies (such as Taihu Lake and the Yangtze River Estuary) achieved PUs of $> 10\%$ (greenish to reddish), and the PUs for smaller lakes (Shiji Lake, Nanyi Lake and Chaohu Lake) were generally $> 5\%$ (light bluish to greenish). A large portion of the Yangtze River channel in

region 1 also showed high $R_{rs_rrc-1240}$ PUs of $> 10\%$, while the corresponding R_{rs_swir} PUs were generally $< 2\%$. Noticeably, when no R_{rs_swir} data coverage was found for several water bodies (such as Gu-cheng, Chenghu, Caohu, and parts of the Yangtze River channel, circled in red), $R_{rs_rrc-1240}$ provided new usable data.

The PUs also showed significant seasonality, which can be visualized through the climatological monthly mean PUs (i.e., the mean value of the monthly mean PUs for a given month throughout the observation period) in January and June (Fig. 6). The January PUs appeared to be more than one degree of magnitude higher than those in June for both R_{rs_swir} and $R_{rs_rrc-1240}$. Numerically, for R_{rs_swir} and $R_{rs_rrc-1240}$, the mean PUs were 2.4% and 15.5%, respectively, in January but 1.0% and 7.7%, respectively, in June. Similar to the results for the entire period, $R_{rs_rrc-1240}$ exhibited significantly higher PUs than R_{rs_swir} . The pronounced data coverage advantage of $R_{rs_rrc-1240}$ in region 1 appeared to be true for all climatological months. As demonstrated in Table 2 & Fig. 7, the mean PUs of $R_{rs_rrc-1240}$ were nearly one order of magnitude higher than those of R_{rs_swir} , and the ratio between the two ranged from 6.0 in February to 10.1 in April. While the largest PUs were found in December for R_{rs_swir} and $R_{rs_rrc-1240}$, the minimum mean PUs occurred in June.

The PUs of the 15-year observation period in region 2 are illustrated in Fig. 8, which clearly reveals the markedly higher chances of obtaining usable $R_{rs_rrc-1240}$ than R_{rs_swir} . The PUs of R_{rs_swir} showed generally low values of $< 1\%$ for the entire region, with a mean value of 0.2%. In contrast, the $R_{rs_rrc-1240}$ not only demonstrated higher mean PUs (3.0%) than R_{rs_swir} but also showed a pronounced increase in data coverage. While usable $R_{rs_rrc-1240}$ data were found in many water bodies, all R_{rs_swir} data were considered low quality and were excluded in the PUs calculations. For example, many lakes and the Yangtze River channel located east of Liangzi Lake (red box) are completely missing from the PUs calculations when using R_{rs_swir} , while usable reflectance products were found in these regions when using $R_{rs_rrc-1240}$.

Seasonal variability of PUs was also observed in region 2, and the monthly mean values in January and June for both R_{rs_swir} and $R_{rs_rrc-1240}$ are presented in Fig. 9. Although the same low mean PUs (0.4%) was found for R_{rs_swir} in these two months, the coverage in June appears to be less than that in January. Similar to the results of the entire period, $R_{rs_rrc-1240}$ not only shows significantly higher PUs than R_{rs_swir} in both months but also exhibits much broader data coverage.

The climatological monthly mean PUs for all 12 months for region 2 were also estimated and plotted (Fig. 7). The mean PUs of $R_{rs_rrc-1240}$ were 3.1–15.4 times larger than those of R_{rs_swir} in region 2, consistent with the patterns shown in region 1. PUs minima for both R_{rs_swir} and $R_{rs_rrc-1240}$ were also found in June in region 2, while the PUs maxima for these two products differed (December for $R_{rs_rrc-1240}$ and July for R_{rs_swir}). Interestingly, while the PUs of region 2 were several degrees

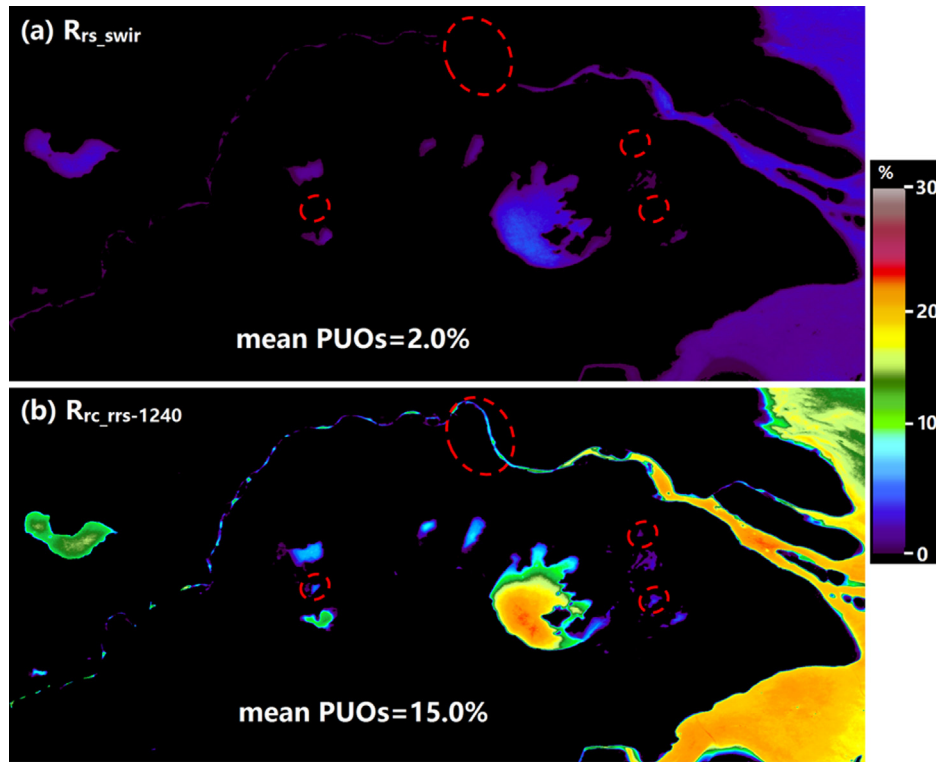


Fig. 5. The percentage of usable observations (PUOs) of R_{rs_swir} (a) and $R_{rs_rrc-1240}$ (b) for region 1 between 2002 and 2016; the mean values of the entire region are also noted. The red circles indicate areas with positive PUOs in $R_{rs_rrc-1240}$ where no valid R_{rs_swir} observations were found.

of magnitude less than those of region 1 for both R_{rs_swir} and $R_{rs_rrc-1240}$, the mean PUOs of $R_{rs_rrc-1240}$ in region 2 appeared to be comparable or even higher than the PUOs of R_{rs_swir} depending on the month.

4.3. Agreement with in situ spectral data

In general, $R_{rs_rrc-1240}$ demonstrated significantly higher correlations (R^2) with the in situ R_{rs} data than R_{rs_swir} for most MODIS spectral bands (see Table 3). Two bands (412 nm and 859 nm) showed slightly poorer correlations between $R_{rs_rrc-1240}$ and the in situ data than between R_{rs_swir} and the in situ data. Comparable or smaller RMSDs were found between R_{rs_swir} and the in situ data than between R_{rs_swir} and the in situ data except for the 412-nm and 859-nm bands. The mean/median ratios showed patterns that were similar to that of the RMSD and R^2 values,

where the proximities to 1 were comparable between R_{rs_swir} and $R_{rs_rrc-1240}$ for the blue bands. The in situ data were collected from various inland and coastal waters and represented different water optical features. Thus, the validation with field measurements indicates that the usable $R_{rs_rrc-1240}$ performs similarly to R_{rs_swir} when used for ocean color applications, while the PUOs of the R_{rc} -converted reflectance appear to be much higher than those of the R_{rs_swir} .

5. Discussion

5.1. Factors affecting PUOs

The $R_{rs_rrc-1240}$ demonstrated much higher PUOs than R_{rs_swir} for all seasons and regions. Such disparities may be primarily due to the

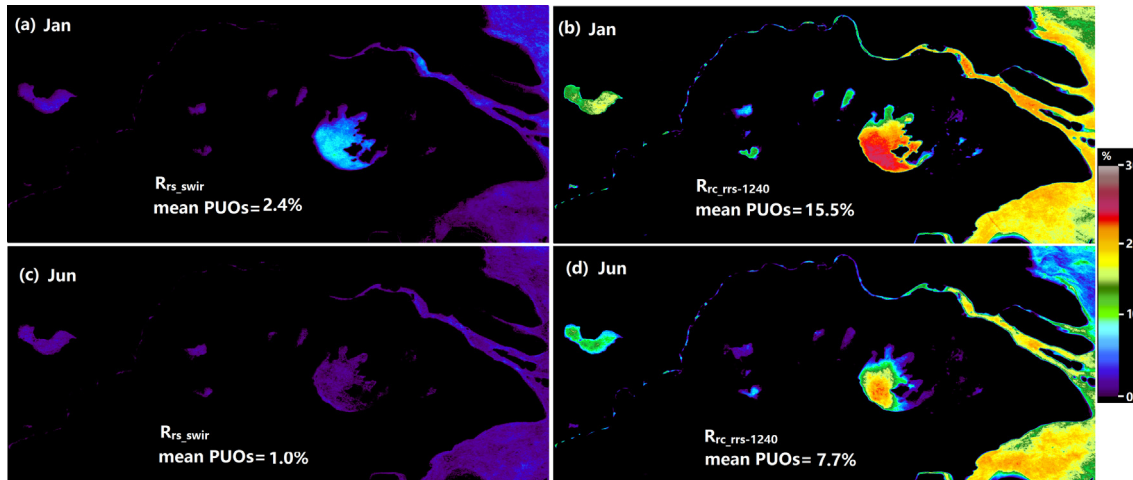


Fig. 6. The percentages of usable observations (PUOs) of R_{rs_swir} and $R_{rs_rrc-1240}$ in region 1 for two different climatological months; the mean values of the entire region are also noted.

Table 2

Comparisons of the percentage of usable observations (PUOs) between $R_{rc_rrs-1240}$ and R_{rs_swir} for different climatological months and regions (the data in parentheses are the standard deviations in the region). The ratios between the two PUOs are also estimated.

	Region 1			Region 2		
	$R_{rc_rrs-1240}$ (%)	R_{rs_swir} (%)	Ratio	$R_{rc_rrs-1240}$ (%)	R_{rs_swir} (%)	Ratio
Jan	15.5 (5.7)	2.4 (2.0)	6.4	2.9 (2.8)	0.4 (0.3)	7.0
Feb	12.9 (5.2)	2.2 (1.9)	6.0	1.7 (1.5)	0.4 (0.3)	4.3
Mar	18.4 (7.7)	2.6 (1.5)	7.1	2.1 (1.6)	0.5 (0.4)	3.9
Apr	16.1 (7)	1.6 (0.8)	10.1	1.7 (1.4)	0.5 (0.4)	3.2
May	14.5 (6.6)	1.8 (0.9)	8.2	1.5 (1.2)	0.5 (0.3)	3.1
Jun	7.7 (4.3)	1.0 (0.5)	7.8	1.3 (1)	0.4 (0.2)	3.6
Jul	12.9 (7.2)	2.4 (1.2)	5.5	3.9 (3)	0.7 (0.6)	5.6
Aug	13.8 (7.1)	2.3 (1.1)	6.1	4.8 (3.6)	0.6 (0.5)	8.2
Sep	13.7 (6.3)	1.7 (0.8)	7.9	4.8 (3.4)	0.6 (0.5)	7.5
Oct	19.8 (8)	2.8 (1.4)	7.0	5.8 (4.1)	0.4 (0.2)	15.4
Nov	17.9 (6.5)	2.7 (1.5)	6.7	4.9 (3.7)	0.4 (0.3)	11.8
Dec	22.8 (8.4)	3.5 (2.8)	6.5	5.5 (4.7)	0.5 (0.4)	10.4
Mean	15.5 (3.9)	2.3 (0.7)	7.1	3.4 (1.7)	0.5 (0.1)	7.0

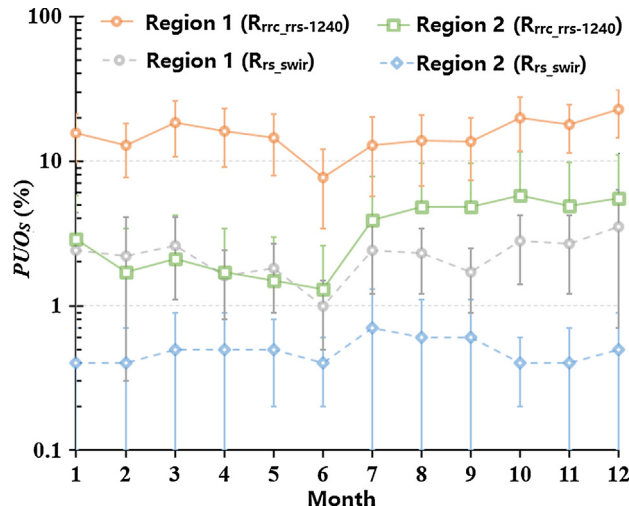


Fig. 7. The comparison of the regional mean percentage of usable observations (PUOs) between R_{rs_swir} and $R_{rs_rrc-1240}$ for different climatological months in the two regions.

differences in AC procedures. The R_{rs_swir} products were generated using a sophisticated AC scheme, where the aerosol contributions to the TOA signals were first derived using two SWIR bands (1240 nm and 2130 nm) with an assumption of zero reflection in these bands. Then, the derived aerosol information was extrapolated into shorter visible-to-NIR wavelengths to remove the aerosol effects. The accuracy of R_{rs_swir} strongly depends on the performances of the two SWIR bands. Perturbations in either SWIR band not only impact the magnitude of the preliminarily derived aerosol signals of the SWIR bands but also lead to problematic aerosol extrapolations in other bands. As such, low-quality R_{rs_swir} retrievals are expected for waters close to land, with potential problems in terms of both spectral shape and magnitude. Indeed, for inland or coastal waters, the signals of SWIR bands are prone to contamination from nearby land surfaces (i.e., LAEs). Land reflection can be significantly higher than water reflection, leading to errors in reflectance products when the SWIR-based AC method is used. In contrast, aerosol correction of $R_{rs_rrc-1240}$ is only one step of Rayleigh reflectance subtraction in 1240-nm band. Although the 1240-nm band is not immune to LAEs, a single subtraction does not significantly change the spectral shape of the resulting $R_{rs_rrc-1240}$. In addition, the error introduced by the assumption of white aerosols is much simpler than the inappropriate extrapolations based on the two SWIR bands (Wang

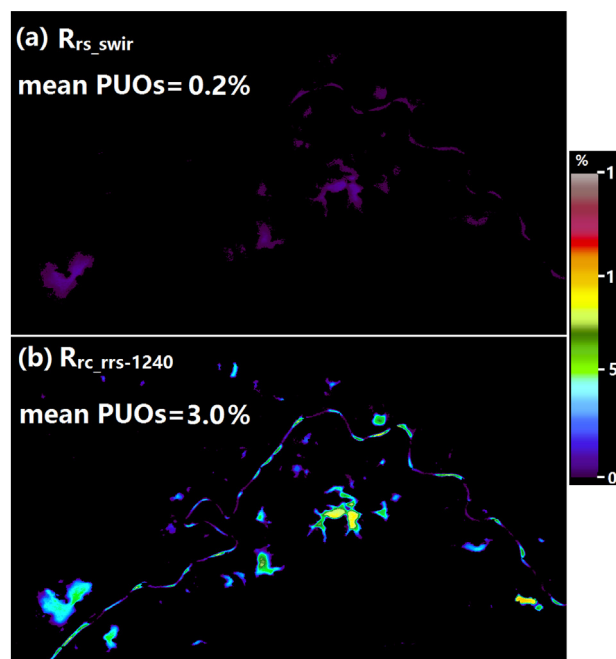


Fig. 8. The percentages of usable observations (PUOs) of R_{rs_swir} (a) and $R_{rs_rrc-1240}$ (b) for region 2 between 2002 and 2016; the mean values of the entire region are also noted. The various water bodies in the red box showed positive PUOs in $R_{rs_rrc-1240}$, whereas no valid R_{rs_swir} observations were found in these areas except in several large lakes.

and Shi, 2007). As LAEs increase with increasing wavelength, the 2130-nm band tends to be more influenced by LAEs than the 1240-nm band, leading to the greater reduction in the PUOs of R_{rs_swir} than those of $R_{rs_rrc-1240}$.

The discrepancies in PUOs between different regions or water bodies can also be attributed to LAEs. Numerically, the relationship between the mean PUOs (over 2002–2016) of $R_{rs_rrc-1240}$ and lake surface area (see lake sizes in Table S1) can be described as a power function (see Fig. 10), where the PUOs increase significantly with increasing lake size. A similar power function relation was also found for R_{rs_swir} , but the magnitude was much smaller than that of $R_{rs_rrc-1240}$. These patterns occur because LAEs impact only land-adjacent pixels, and these effects decrease dramatically with increasing distance from the coastline. Therefore, the percentages of pixels that are affected by LAEs in large water bodies (such as Taihu Lake and the Yangtze River Estuary) are less than those in small lakes and narrow river channels. In addition to lake size, the morphology of the lake boundaries can also impact the severity of the LAEs, and this could partially explain the discrete points in the scatter plots in Fig. 9 (Feng and Hu, 2017).

The seasonality of the PUOs is likely to be associated with the seasonal changes in the presence of clouds and sunglint. The rainy season in the Yangtze Plain area is between April and June each year (Feng et al., 2014a), and the chances of cloud occurrence and lower PUOs during these months are high. In contrast, the months with high PUOs correspond to the dry season with minimum precipitation. In addition, the MODIS sensors do not have a tilting capability like SeaWiFS; thus, a considerable number of MODIS observations could be contaminated by sunglint (Feng and Hu, 2015). Such influences are prominent in the summer months due to the decreased solar zenith angle in the Yangtze River Basin area, leading to PUOs minima in June in many regions for many reflectance products.

5.2. Limitations and future efforts

The replacement of R_{rs_swir} with $R_{rc_rrc-1240}$ in ocean color applications would yield a pronounced increase in usable data. We

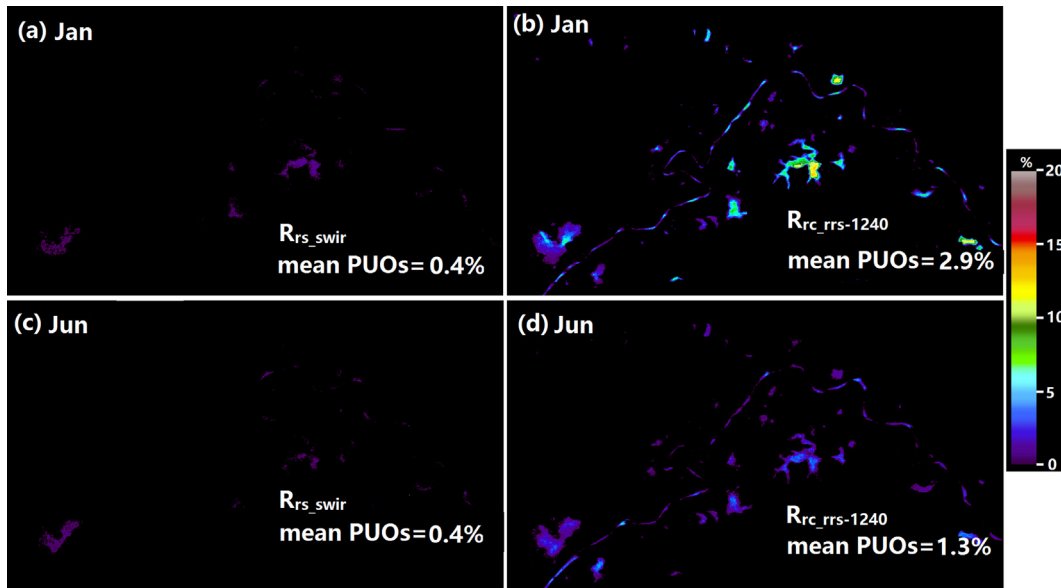


Fig. 9. The percentages of usable observations (PUOs) of R_{rs_swir} and $R_{rc_rrc-1240}$ in region 2 for two different climatological months; the mean values of the entire region are noted.

Table 3

The accuracy measures of R_{rs_swir} and $R_{rc_rrc-1240}$ for different MODIS bands gauged with field spectral measurements; the number of points used in the validations are listed in the last column.

	Wavelength	R^2	RMSD	Mean ratio	Median ratio	n_points
R_{rs_swir}	412	0.03	77.18%	0.38	0.44	78
	443	0.00	63.24%	0.50	0.56	86
	469	0.00	62.35%	0.51	0.57	94
	488	0.00	56.21%	0.55	0.59	95
	531	0.01	46.13%	0.64	0.64	79
	547	0.27	58.81%	0.51	0.59	26
	555	0.03	48.24%	0.61	0.62	107
	645	0.21	46.32%	0.65	0.68	107
	667	0.08	78.98%	0.41	0.52	16
	678	0.10	76.65%	0.46	0.60	21
	748	0.14	54.23%	0.64	0.67	29
	859	0.16	51.97%	0.74	0.80	112
	869	0.05	75.94%	0.46	0.56	40
$R_{rc_rrc-1240}$	412	0.09	82.25%	0.18	0.17	78
	443	0.31	63.17%	0.38	0.35	86
	469	0.17	54.42%	0.47	0.44	94
	488	0.18	49.81%	0.52	0.49	95
	531	0.42	39.01%	0.63	0.63	79
	547	0.55	48.40%	0.53	0.49	26
	555	0.10	36.01%	0.68	0.66	107
	645	0.32	36.57%	0.76	0.73	107
	667	0.01	56.12%	0.52	0.54	16
	678	0.06	56.84%	0.54	0.50	21
	748	0.58	59.36%	0.44	0.50	29
	859	0.17	145.75%	0.94	0.62	112
	869	0.32	77.72%	0.30	0.39	40

acknowledge that the subtraction of $R_{rc,1240}$ from all MODIS bands is certainly not a perfect AC method, as aerosol reflectance is not spectrally independent and the spectral slope is defined by the Angstrom exponent (Gordon, 1997). Therefore, the aerosol-associated uncertainties in $R_{rc_rrc-1240}$ tend to be enhanced in blue bands relative to green-to-NIR bands, due to the larger differences in wavelength and thus the associated aerosol reflection. This observation also explains the poorer agreements of Best-Quality R_{rs_swir} and $R_{rc_rrc-1240}$ for the blue/green bands than for longer wavelengths (Figs. 3 and 4). Thus, an improved correction method needs to be developed to remove the residual

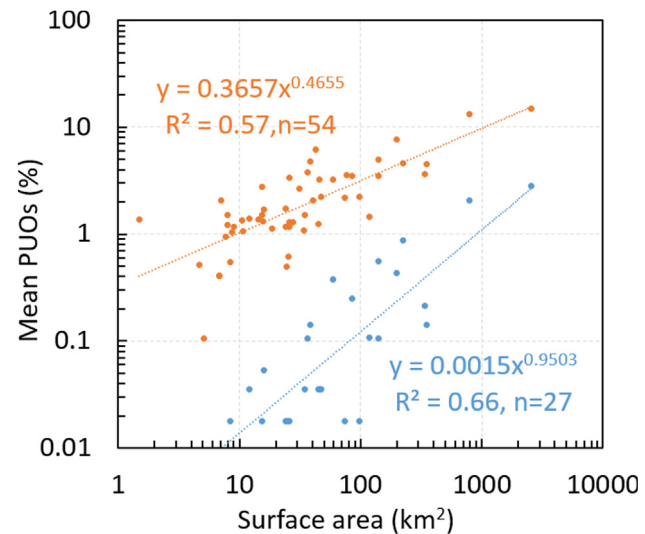


Fig. 10. Correlations between mean PUOs (2002–2016) of $R_{rc_rrc-1240}$ and lake surface areas for both R_{rs_swir} and $R_{rc_rrc-1240}$.

aerosol contamination in these bands and to account for the spectral dependency of the aerosol reflectance.

LAEs appeared to be the primary reason for the low PUOs of R_{rs_swir} for inland waters and coastal oceans, as the two SWIR bands for AC are susceptible to these forms of contamination. A recent look-up table (LUT)-based method presented by Feng and Hu (2017) can be used to correct LAEs, and preliminary tests showed significant improvements in both data quality and quantity of R_{rs} retrievals. While this method was proposed based on simple land/water morphology (i.e., a long and straight Madagascar coastline), its implementation and operational use for the same study region are not trivial, and its applications in other areas with more complex morphological features require further evaluations. An additional difficulty of the method is that the LAE correction requires considerable amounts of processing resources. Indeed, once an operational LAE correction method is developed to improve the PUOs of R_{rs_swir} , the advantages of $R_{rs_rrc-1240}$ in PUOs would be significantly diminished.

5.3. Implications for ocean color applications

After the simple removal of aerosol contributions, R_{rc} exhibited good agreement with R_{rs_swir} for most MODIS bands, and the data were selected as the Best-Quality reflectance through an objective QA scoring system. Any R_{rc} spectrum can be converted into remote sensing reflectance (i.e., $R_{rs_rrc-1240}$) using the established correlations between $R_{rc-1240}$ and R_{rs_swir} (Table 1). As the subtraction of Rayleigh reflectance at 1240 nm is more tolerant of environmental perturbations than the complicated SWIR-based aerosol correction algorithm (Wang and Shi, 2007), a remarkable increase in valid observations can be expected with the use of $R_{rs_rrc-1240}$. Indeed, $R_{rs_rrc-1240}$ showed PUs that were several times to more than one order of magnitude higher than those of R_{rs_swir} . The quality of the usable $R_{rs_rrc-1240}$ data was not only guaranteed by the QA scoring system (50% of the spectral bands fell within the upper/lower boundaries of certain predefined water types) but also confirmed with in situ spectral measurements from various water bodies. Although the performance of $R_{rs_rrc-1240}$ in the NIR bands could not be evaluated with the QA system due to the lack of reference spectra (Wei et al., 2016), the validity of these bands was verified through the reliable spectral shapes of the shorter wavelengths as well as the consistency with the in situ measurements.

Ocean color applications could significantly benefit from such an impressive increase in PUs, not only through the increased capability of tracking short-term variability but also through the newly offered possibility for monitoring small water bodies. Fig. 11 shows the total number of valid observations from two MODIS bands for each season between 2002 and 2006 for three lakes with different surface areas. A valid observation is defined as a pixel with a QA score > 0.5 and a reflectance in the examined band that is not zero. Each point represents the mean total number of observations in a 3×3 window centered over the lake, and the LAEs were considered to be the minimum in the lake. Similar to previous comparisons, the overwhelming data volume advantages of $R_{rs_rrc-1240}$ are clearly demonstrated for all three lakes, and

the number of valid observations tends to increase with increasing lake size. Obviously, the use of $R_{rs_rrc-1240}$ is expected to produce more statistically meaningful long-term trends than R_{rs_swir} .

Another interesting finding is that R_{rs_swir} in the 555-nm band appears to have difficulty in producing continuous high-quality data for small lakes, such as Liangzi and Dong Lake. In particular, R_{rs_swir} generally did not yield any valid measurements in the 555-nm band during the entire observation period. In contrast, $R_{rs_rrc-1240}$ in the same band provided continuous usable observations from 2002 to 2016 for all three lakes (except for several seasons in Dong Lake and Liangzi Lake), despite the significant differences in surface areas (two orders of magnitude). When available, the PUs of ocean bands were comparable to those of land bands for Liangzi and Donghu Lake, while the saturation problem led to serious missing data problems in the turbid Taihu Lake, particularly during dry seasons when the water clarity was especially low (Hou et al., 2017).

The remarkable data recovery could be further demonstrated by the mean PUs (over 2002–2016) of $R_{rc_rrc-1240}$ and R_{rs_swir} for 54 lakes in both regions (see Fig. 12). Half of the examined lakes demonstrated PUs of 0% for R_{rs_swir} during the entire observation period. The remaining lakes, although with non-zero PUs values, also yielded very limited usable R_{rs_swir} data (red bars). For example, the maximum PUs of R_{rs_swir} was < 3% (Taihu Lake), and the PUs for the other lakes were much lower. In contrast, $R_{rc_rrc-1240}$ products were available for all 54 lakes, and nearly 50% of the lakes showed mean PUs of > 3%. The relative differences (represented as $PUs[(R_{rc_rrc-1240}-R_{rs_swir})/R_{rc_rrc-1240}]$) further illustrated the prevailing PUs advantage of $R_{rc_rrc-1240}$, as the differences were > 80% (mostly > 95%), suggesting that the mean PUs of $R_{rc_rrc-1240}$ for these lakes were at least 5 times greater than those of R_{rs_swir} . Indeed, the newly recovered datasets could open up new possibilities for monitoring water quality across a number of inland systems at the entire basin scale. In contrast, R_{rs_swir} provides effective observations only for relatively large water bodies, prohibiting a comprehensive assessment of water status in the study region.

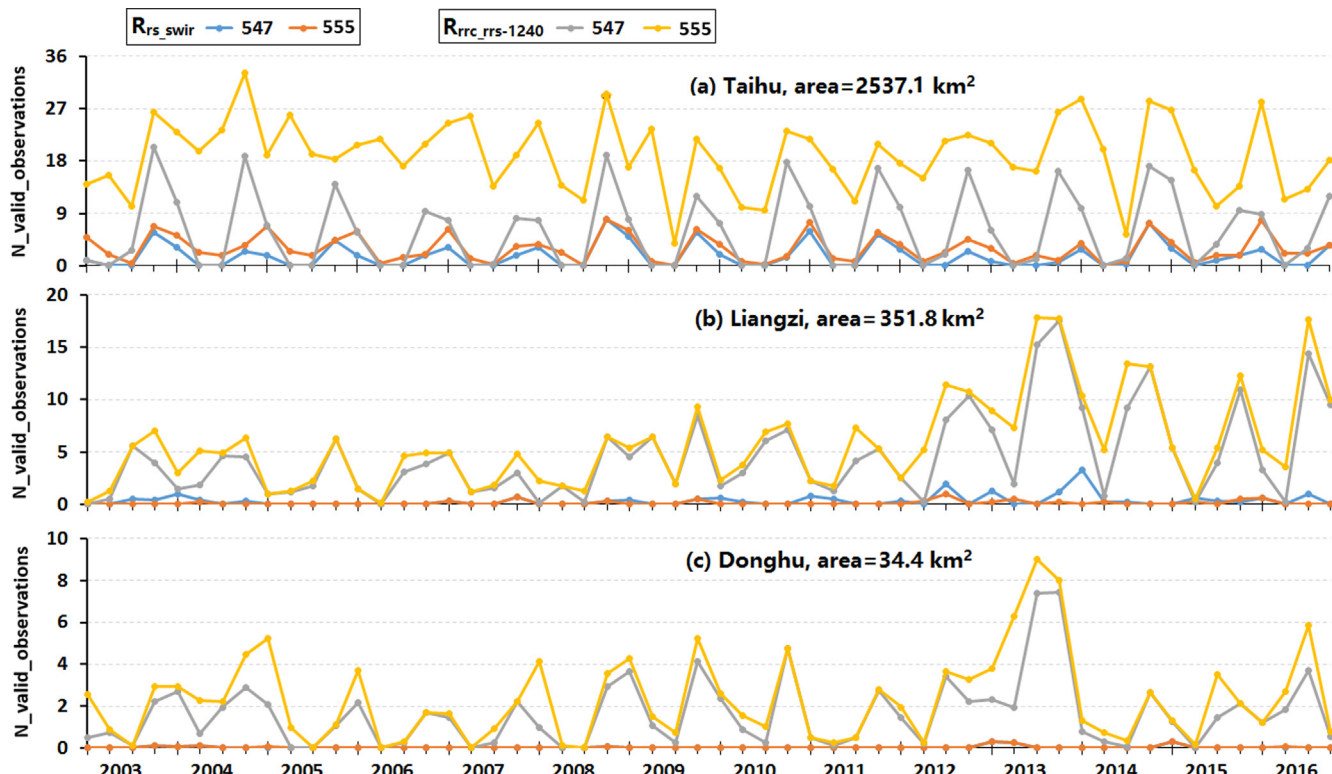


Fig. 11. The number of valid observations in two red bands (547 and 555 nm) for each season between 2002 and 2016 for three lakes with different surface areas (the names and surface areas are noted in each panel). The results for two different reflectance products (R_{rs_swir} and $R_{rs_rrc-1240}$) are compared.

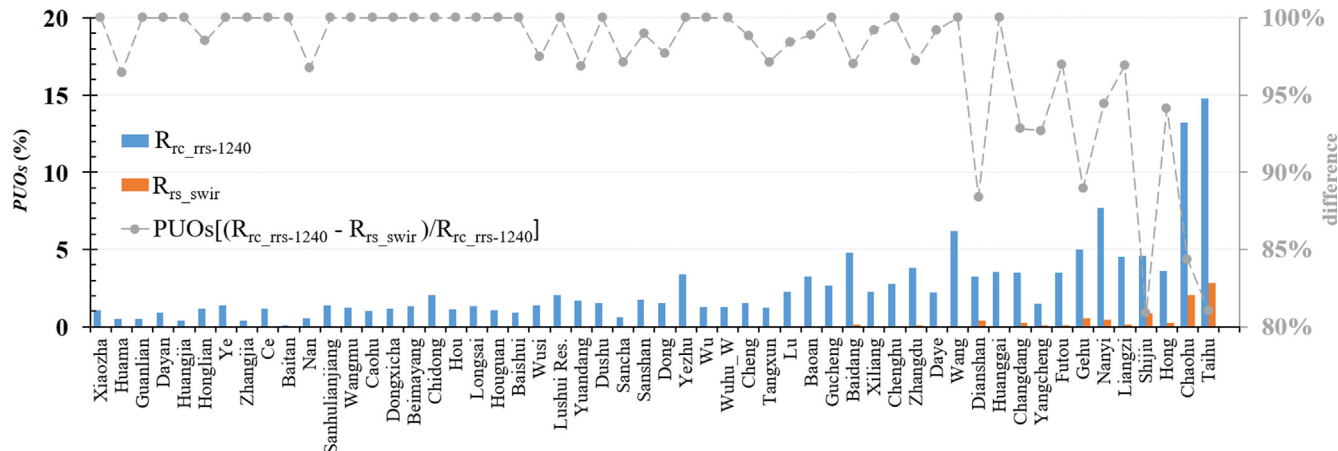


Fig. 12. The comparisons of the mean PUOs (2002–2016) for $R_{rc_rrs-1240}$ and R_{rs_swir} for 54 lakes in the two study regions; the relative differences between the two products are also plotted (represented as the PUOs $[(R_{rc_rrs-1240}-R_{rs_swir})/R_{rc_rrs-1240}]$).

6. Conclusion

The correlations between the Best-Quality R_{rc} and R_{rs_swir} products were examined in areas where the data were passed the objective QA system. A simple subtraction of $R_{rc,1240}$ (i.e., $R_{rc-1240}$) resulted in significantly improved relationships between R_{rc} and R_{rs_swir} . The R^2 values between $R_{rc,1240}$ and R_{rs_swir} were > 0.5 for all MODIS green-to-NIR wavelengths, and the red-to-NIR bands showed higher R^2 values of > 0.85 . Such significant correlations enable the substitution of $R_{rc,1240}$ ($R_{rc,1240}$ -converted reflectance data using the established correlations with R_{rs_swir}) for R_{rs_swir} in water color applications. The fidelity of usable $R_{rc_rrs-1240}$ was confirmed not only by the QA system but also by validation with in situ measurements from various water bodies. It is acknowledged that an advanced AC method is still needed to account for the spectral dependency of aerosol reflectance to improve the simple subtraction of $R_{rc,1240}$ from all bands in the current study.

The most significant finding of this study is the remarkable increase in PUOs for $R_{rc_rrs-1240}$, as the PUOs of $R_{rc_rrs-1240}$ could be several times to more than one order of magnitude higher than those of R_{rs_swir} in the study regions. Additionally, the PUOs exhibited power function growth with increasing lake size for both $R_{rc_rrs-1240}$ and R_{rs_swir} . The interferences of LAEs on the SWIR bands appeared to be the reason for not only the discrepancy in PUOs between $R_{rc_rrs-1240}$ and R_{rs_swir} but also the correlations between PUOs and lake surface area.

It is believed that ocean color applications in the studied regions could substantially benefit from the impressive increase in valid observations. However, the use of the established relationship between $R_{rc-1240}$ and R_{rs_swir} in other water bodies still requires caution, unless these water bodies share similar optical features and aerosol conditions with the study regions. Notably, this study was not intended to demonstrate the superiority of Rayleigh correction over full atmospheric correction methods (i.e., SWIR- or NIR-based methods); instead, it demonstrated the necessity of improving the SWIR-based AC algorithm through the correction of LAEs to achieve better data accuracy and coverage for small water bodies. Finally, the methods proposed here are extendable to other instruments (e.g., MODIS Terra, Suomi NPP-VIIRS, and MERIS) to examine the possibility of replacing fully corrected R_{rs} with R_{rc} -converted reflectance products in coastal and inland water applications.

Acknowledgements

This work was supported by the National Natural Science Foundation of China (Nos: 41671338, 41401388 and 41331174), Guan the Youth Innovation Promotion Association of Chinese Academy of Sciences (2015128), and the Key Program of the Chinese Academy of

Sciences (ZDRW-ZS-2017-3-4). Additional support was provided by the Southern University of Science and Technology (Grant No. G01296001). The MODIS data were provided by US NASA via their website at <https://oceancolor.gsfc.nasa.gov/>.

Appendix A. Supplementary material

Supplementary data associated with this article can be found, in the online version, at <https://doi.org/10.1016/j.isprsjprs.2018.08.020>.

References

- Bailey, S.W., Werdell, P.J., 2006. A multi-sensor approach for the on-orbit validation of ocean color satellite data products. *Remote Sens. Environ.* 102, 12–23.
- Budiman, S., Suhyb Salama, M., Vekerdy, Z., Verhoeft, W., 2012. Deriving optical properties of Mahakam Delta coastal waters, Indonesia using in situ measurements and ocean color model inversion. *ISPRS J. Photogramm. Remote Sens.* 68, 157–169.
- Chander, G., Markham, B.L., Helder, D.L., 2009. Summary of current radiometric calibration coefficients for Landsat MSS, TM, ETM+, and EO-1 ALI sensors. *Remote Sens. Environ.* 113, 893–903.
- Duan, H., Feng, L., Ma, R., Zhang, Y., Loiselle, S.A., 2014. Variability of particulate organic carbon in inland waters observed from MODIS Aqua imagery. *Environ. Res. Lett.* 9, 084011.
- Feng, L., Hu, C., 2015. Comparison of Valid Ocean Observations between MODIS Terra and Aqua over the Global Oceans. *IEEE Trans. Geosci. Remote Sens.* 1–11.
- Feng, L., Hu, C., 2016. Cloud adjacency effects on top-of-atmosphere radiance and ocean color data products: a statistical assessment. *Remote Sens. Environ.* 174, 301–313.
- Feng, L., Hu, C., 2017. Land adjacency effects on MODIS Aqua top-of-atmosphere radiance in the shortwave infrared: Statistical assessment and correction. *J. Geophys. Res.: Oceans*.
- Feng, L., Hu, C., Chen, X., Song, Q., 2014a. Influence of the three Gorges Dam on total suspended matters in the Yangtze Estuary and its adjacent coastal waters: Observations from MODIS. *Remote Sens. Environ.* 140, 779–788.
- Feng, L., Hu, C., Chen, X., Tian, L., Chen, L., 2012. Human induced turbidity changes in Poyang Lake between 2000 and 2010: Observations from MODIS. *J. Geophys. Res.: Oceans* 117.
- Feng, L., Hu, C., Han, X., Chen, X., Qi, L., 2014b. Long-term distribution patterns of chlorophyll-a concentration in China's largest freshwater lake: MERIS full-resolution observations with a practical approach. *Remote Sens.* 7, 275–299.
- Feng, L., Hu, C., Li, J., 2018. Can MODIS land reflectance products be used for estuarine and inland waters? *Water Resour. Res.* 54, 3583–3601. <https://doi.org/10.1029/2017WR021607>.
- Gordon, H.R., 1997. Atmospheric correction of ocean color imagery in the Earth Observing System era. *J. Geophys. Res.* 102, 17081–17106.
- Gordon, H.R., Wang, M., 1994. Retrieval of water-leaving radiance and aerosol optical thickness over the oceans with SeaWiFS: a preliminary algorithm. *Appl. Opt.* 33, 443–452.
- Hale, G.M., Querry, M.R., 1973. Optical constants of water in the 200-nm to 200-μm wavelength region. *Appl. Opt.* 12, 555–563.
- Harding Jr, L.W., Magnuson, A., Mallonee, M.E., 2005. SeaWiFS retrievals of chlorophyll in Chesapeake Bay and the mid-Atlantic bight. *Estuar. Coast. Shelf Sci.* 62, 75–94.
- Hou, X., Feng, L., Duan, H., Chen, X., Sun, D., Shi, K., 2017. Fifteen-year monitoring of the turbidity dynamics in large lakes and reservoirs in the middle and lower basin of the Yangtze River, China. *Remote Sens. Environ.* 190, 107–121.
- Hu, C., 2009. A novel ocean color index to detect floating algae in the global oceans. *Remote Sens. Environ.* 113, 2118–2129.

- Hu, C., Carder, K.L., Muller-Karger, F.E., 2000. Atmospheric correction of SeaWiFS imagery over turbid coastal waters: a practical method. *Remote Sens. Environ.* 74, 195–206.
- Hu, C., Feng, L., Lee, Z., Davis, C.O., Mannino, A., McClain, C.R., Franz, B.A., 2012. Dynamic range and sensitivity requirements of satellite ocean color sensors: learning from the past. *Appl. Opt.* 51, 6045–6062.
- Jamet, C., Loisel, H., Kuchinke, C.P., Ruddick, K., Zibordi, G., Feng, H., 2011. Comparison of three SeaWiFS atmospheric correction algorithms for turbid waters using AERONET-OC measurements. *Remote Sens. Environ.* 115, 1955–1965.
- Kaufman, Y., Tanré, D., Remer, L.A., Vermote, E., Chu, A., Holben, B., 1997. Operational remote sensing of tropospheric aerosol over land from EOS moderate resolution imaging spectroradiometer. *J. Geophys. Res.: Atmosph.* 102, 17051–17067.
- Li, J., Hu, C., Shen, Q., Barnes, B.B., Murch, B., Feng, L., Zhang, M., Zhang, B., 2017. Recovering low quality MODIS-Terra data over highly turbid waters through noise reduction and regional vicarious calibration adjustment: A case study in Taihu Lake. *Remote Sens. Environ.* 197, 72–84.
- Li, J., Wang, S., Wu, Y., Zhang, B., Chen, X., Zhang, F., Shen, Q., Peng, D., Tian, L., 2016. MODIS observations of water color of the largest 10 lakes in China between 2000 and 2012. *Int. J. Digital Earth* 9, 788–805.
- Markham, B.L., Dabney, P.W., Storey, J.C., Morfitt, R., Knight, E., Kvaran, G., Lee, K., 2008. Landsat Data Continuity Mission Calibration and Validation.
- Mobley, C.D., 1999. Estimation of the remote-sensing reflectance from above-surface measurements. *Appl. Opt.* 38, 7442–7455.
- Mouw, C.B., Greb, S., Aurin, D., DiGiacomo, P.M., Lee, Z., Twardowski, M., Binding, C., Hu, C., Ma, R., Moore, T., 2015. Aquatic color radiometry remote sensing of coastal and inland waters: challenges and recommendations for future satellite missions. *Remote Sens. Environ.* 160, 15–30.
- Mueller, J.L., McClain, G.S.F.C.R., Mueller, J., Bidigare, R., Trees, C., Balch, W., Dore, J., Drapeau, D., Karl, D., Van, L., 2003. Ocean Optics Protocols for Satellite Ocean Color Sensor Validation, Revision 5, Volume V: Biogeochemical and Bio-Optical Measurements and Data Analysis Protocols. National Aeronautical and Space Administration Report, vol. 21621, pp. 1–72.
- Novoa, S., Doxaran, D., Ody, A., Vanhellemont, Q., Lafon, V., Lubac, B., Gernez, P., 2017. Atmospheric corrections and multi-conditional algorithm for multi-sensor remote sensing of suspended particulate matter in low-to-high turbidity levels coastal waters. *Remote Sens.* 9, 61.
- Petus, C., Chust, G., Gohin, F., Doxaran, D., Froidefond, J.-M., Sagarminaga, Y., 2010. Estimating turbidity and total suspended matter in the Adour River plume (South Bay of Biscay) using MODIS 250-m imagery. *Cont. Shelf Res.* 30, 379–392.
- Petus, C., Marieu, V., Novoa, S., Chust, G., Bruneau, N., Froidefond, J.-M., 2014. Monitoring spatio-temporal variability of the Adour River turbid plume (Bay of Biscay, France) with MODIS 250-m imagery. *Cont. Shelf Res.* 74, 35–49.
- Ruddick, K.G., Ovidio, F., Rijkeboer, M., 2000. Atmospheric correction of SeaWiFS imagery for turbid coastal and inland waters. *Appl. Opt.* 39, 897–912.
- Siegel, D.A., Wang, M., Maritorena, S., Robinson, W., 2000. Atmospheric correction of satellite ocean color imagery: the black pixel assumption. *Appl. Opt.* 39, 3582–3591.
- Son, Y.-S., Kim, H.-C., 2018. Empirical ocean color algorithms and bio-optical properties of the western coastal waters of Svalbard, Arctic. *ISPRS J. Photogramm. Remote Sens.* 139, 272–283.
- Stumpf, R., Arnone, R., Gould, R., Martinolich, P., Ransibrahmanakul, V., 2003. A partially coupled ocean-atmosphere model for retrieval of water-leaving radiance from SeaWiFS in coastal waters. *NASA Tech. Memo* 2006892, 51–59.
- Sun, D., Li, Y., Le, C., Shi, K., Huang, C., Gong, S., Yin, B., 2013. A semi-analytical approach for detecting suspended particulate composition in complex turbid inland waters (China). *Remote Sens. Environ.* 134, 92–99.
- Vanhellemont, Q., Ruddick, K., 2015. Advantages of high quality SWIR bands for ocean colour processing: Examples from Landsat-8. *Remote Sens. Environ.* 161, 89–106.
- Wang, M., Shi, W., 2006. Cloud masking for ocean color data processing in the coastal regions. *IEEE Trans. Geosci. Remote Sens.* 44 3196–3105.
- Wang, M., Shi, W., 2007. The NIR-SWIR combined atmospheric correction approach for MODIS ocean color data processing. *Opt. Express* 15, 15722–15733.
- Wang, M., Shi, W., 2012. Sensor noise effects of the SWIR bands on MODIS-derived ocean color products. *IEEE Trans. Geosci. Remote Sens.* 50, 3280–3292.
- Wang, M., Tang, J., Shi, W., 2007. MODIS-derived ocean color products along the China east coastal region. *Geophys. Res. Lett.* 34.
- Wei, J., Lee, Z., Shang, S., 2016. A system to measure the data quality of spectral remote-sensing reflectance of aquatic environments. *J. Geophys. Res. (Oceans)* 121, 8189–8207.
- Werdell, P.J., Bailey, S.W., 2005. An improved in-situ bio-optical data set for ocean color algorithm development and satellite data product validation. *Remote Sens. Environ.* 98, 122–140.
- Zhang, B., Li, J., Shen, Q., Chen, D., 2008. A bio-optical model based method of estimating total suspended matter of Lake Taihu from near-infrared remote sensing reflectance. *Environ. Monit. Assess.* 145, 339–347.
- Zhang, F., Li, J., Shen, Q., Zhang, B., Wu, C., Wu, Y., Wang, G., Wang, S., Lu, Z., 2015. Algorithms and schemes for chlorophyll a estimation by remote sensing and optical classification for Turbid Lake Taihu, China. *IEEE J. Sel. Top. Appl. Earth Obs. Remote Sens.* 8, 350–364.
- Zhang, M., Ma, R., Li, J., Zhang, B., Duan, H., 2014. A Validation Study of an Improved SWIR Iterative Atmospheric Correction Algorithm for MODIS-Aqua Measurements in Lake Taihu, China. *IEEE Trans. Geosci. Remote Sens.* 52, 4686–4695.
- Zhang, Y., Ma, R., Duan, H., Loiselle, S., Zhang, M., Xu, J., 2016. A novel MODIS algorithm to estimate chlorophyll a concentration in eutrophic turbid lakes. *Ecol. Ind.* 69, 138–151.